IEEE Journal of Microwaves

Received 26 March 2021; revised 21 April 2021; accepted 3 May 2021. Date of publication 10 June 2021; date of current version 7 July 2021.

Digital Object Identifier 10.1109/JMW.2021.3079205

Stability and Oscillation Analysis at Circuit Level and Through Semi-Analytical Formulations

ALMUDENA SUÁREZ (Fellow, IEEE), SERGIO SANCHO (Member, IEEE), FRANCO RAMÍREZ (Senior Member, IEEE), AND MABEL PONTÓN (Member, IEEE)

(Invited Paper)

University of Cantabria, 39005 Santander, Spain

CORRESPONDING AUTHOR: ALMUDENA SUÁREZ (e-mail: almudena.suarez@unican.es).

This work was supported by a project under Grant TEC2017-88242-C3-1–R

ABSTRACT Harmonic balance provides steady-state solutions only and has significant shortcomings when addressing oscillatory regimes. As a result, complementary methodologies are required both to ensure the stability of the solution obtained and to design/simulate oscillator circuits. The complexity of the stability analysis increases with the number of active elements and the intricacy of the topology, so there can be uncertainties in the case of complex structures. On the other hand, as recently demonstrated oscillators enable a compact and low-cost implementation of RFID readers and radar systems, which comes at the expense of a more complex performance, very difficult/impossible to simulate with commercial HB. This work presents a review of recent advances on stability and oscillation analysis at circuit level and through semi-analytical formulations. At circuit level, a method for the stability analysis of complex microwave systems is presented, based on the calculation of the characteristic determinant, extracted from the commercial simulator through a judicious partition of the system into simpler blocks. This determinant will be used for the first time to obtain the stability boundaries through a contour-intersection method, able to provide multivalued and disconnected curves. At a semi-analytical level, a realistic numerical model of the standalone oscillator, extracted from HB simulations, is introduced in an analytical formulation that describes the oscillator interaction with other elements. Here it will be applied to a self-injection locked radar, in which the oscillator is injected by its own signal after this signal undergoes propagation and reflection effects. A procedure to determine the stability properties considering the time delay of the signal envelope is presented for the first time. Using the same self-injection concept, a new stabilization method to reduce the phase-noise of an existing oscillator with minimum impact on its original frequency is described.

INDEX TERMS Bifurcation, injection locking, oscillator, stability.

I. INTRODUCTION

Most Microwave designers make use of the harmonic balance method (HB) due to its efficient and accurate handling of distributed elements [1]–[3]. However, HB provides steady-state solutions only and has significant shortcomings when addressing oscillatory regimes [3]–[6]. This is due to the mathematical coexistence of the oscillation with a non-oscillatory solution (the DC solution of a free-running oscillator, for instance [7]) to which the error minimization converges by default [1], [3]–[6]. To be physical, the solution obtained with HB must be stable, which can only be ensured with a complementary stability analysis [8]–[21]. This work presents a review of recent methodologies for stability [22], [23], and oscillation analysis [24]–[26] developed at University of Cantabria. As indicated through the text, it includes several new theoretical contributions with respect to previous publications by the group on the two topics.

The stability of a steady-state solution is analyzed [1], [3], [8] applying a small perturbation of complex frequency s. In the presence of this perturbation, the circuit is formulated linearizing the nonlinear devices about the steady-state solution and evaluating the passive linear elements at s [1], [3], [13]. This provides a homogeneous system, and its natural frequencies are given by the roots of its associated characteristic determinant, depending on s. For a stable behavior, all these roots must be in the left-hand side (LHS) of the complex plane. To avoid dealing with complex frequencies, the Nyquist criterion can be applied to the characteristic determinant [1], [3], [8]. This criterion provides the *difference* between the number of zeroes and poles of the determinant located in the right-hand side (RHS) of the complex plane [27]. Thus, the result will be inconclusive unless the number of RHS poles is known beforehand, which is virtually impossible in practice. When the system is explicitly formulated in terms of the Jacobian matrices of the nonlinearities with respect to their control voltages, there cannot be any poles in the RHS [1], [3], [8]. However, this formulation is only possible in in-house HB, since, as stated, it requires access to the Jacobian matrices. To cope with this problem, the works [9], [14] introduced the Normalized Determinant Function (NDF), which can be calculated in commercial HB. The NDF avoids the undesired coexistence of RHS zeroes and poles but must be calculated at the device intrinsic terminals. Thus, it cannot be rigorously obtained when using black-box device models.

A fully different strategy is the one based on the pole-zero identification of a closed-loop transfer function [15]–[19]. This powerful method relies on the fact that all the closed loop transfer functions that can be defined in a linear system share the same denominator [15]–[19], [27] which agrees with the characteristic determinant. As a result, if there are no exact pole-zero cancellations, the poles (defining the stability properties) will be the same, no matter the transfer function analyzed [15]–[19]. In practice, there can be cancellations/quasi-cancellations of RHS zeroes and poles. This will occur if the transfer function is calculated at nodes/branches with low observability and controllability of the unstable loop(s). To avoid missing instabilities several transfer functions must be analyzed, which may become demanding in complex multi-device structures.

Recently a new method has been introduced [23], which is based on a definition of the characteristic determinant that, by construction, cannot exhibit any RHS poles. Unlike [9], [14], the calculation of this determinant does not require access to the intrinsic device terminals. Instead, it is easily obtained by partitioning the structure in simpler blocks that must be stable under either open circuit (OC) or short circuit (SC) terminations [28], [29]. Due to the small size of the blocks, this OC/SC stability can be reliably verified with conventional pole-zero identification applied to a closed-loop transfer function [15]–[19]. Then, the characteristic determinant is calculated at the ports defined in the partition.

A complementary (and computationally efficient) method to avoid unstable behavior is the calculation of the stability boundaries [1], [3]–[6] in terms of parameters such as the bias voltage or a relevant element value. This will also provide insight into the effect of these parameters on the stability properties. Here the stability boundaries will be obtained (for the first time) applying a bifurcation condition to the newly defined characteristic determinant, which will allow addressing the full circuit structure without any observability limitations.

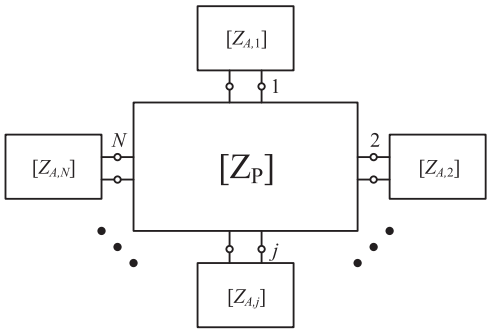

FIGURE 1. Stability analysis through a circuit partition into simpler blocks. The case of OC-stable active blocks is considered. An analogous partition would be carried out in the case of SC-stable blocks, using an admittance description of both the active blocks and the passive linear matrix.

A different goal is the use, instead of the avoidance, of the oscillatory solution to implement compact and low-cost RFID readers and radar systems [30]–[35]. The self-injection locked radar proposed in [33]–[35] enables a simple detection of the target motion through the demodulation of the oscillation frequency, and extensions for range detection using a stepped-frequency modulation [35] have also been proposed. The oscillator is injected by its own signal after this signal undergoes reflection and propagation effects. However, this operation mode often gives rise to multi-valued solutions, virtually impossible to simulate in commercial HB. To cope with this problem, semi-analytical formulations have been introduced [24], [25], [36], which make use of a realistic numerical model of the standalone oscillator, extracted from HB, that is combined with an analytical description of the self-injection loop. Here a new procedure to determine the stability properties considering the time delay of the signal envelope is presented for the first time. Using the same self-injection concept, a new stabilization method to reduce the phase-noise of an existing oscillator with minimum impact on its original free-running frequency is described.

II. CIRCUIT LEVEL STABILITY ANALYSIS OF COMPLEX STRUCTURES

A. SMALL-SIGNAL STABILITY ANALYSIS

The stability analysis proposed in [23] is based on a partition of the structure into N active blocks (containing both active and passive linear elements), connected through a passive linear network (Fig. 1).

The selected N blocks must be stable either under open-circuit (OC) or short-circuit (SC) terminations. One–port active blocks will be considered, though the extension to a

higher number of ports is straightforward. Initially it is assumed that the N one-port active blocks are OC-stable (Fig. 1), so they will be described with their corresponding impedance functions $Z_{A,n}$, where $n = 1 \ldots N$. In turn, the passive linear network will be described with its $N \times N$ impedance matrix $[Z_P]$. The characteristic system is:

$$\left\{ \begin{bmatrix} Z_{A,1}(s) & 0 & \ldots & 0 \\ 0 & Z_{A,2}(s) & \cdots & 0 \\ \vdots & \vdots & \ddots & \vdots \\ 0 & 0 & \ldots & Z_{A,N}(s) \end{bmatrix} + \begin{bmatrix} Z_{P,11}(s) & \ldots & Z_{P,1N}(s) \\ \vdots & \vdots & \vdots \\ Z_{P,N1}(s) & \ldots & Z_{P,NN}(s) \end{bmatrix} \right\} \begin{bmatrix} \Delta I_1 \\ \vdots \\ \Delta I_N \end{bmatrix} = \begin{bmatrix} 0 \\ \vdots \\ 0 \end{bmatrix} \tag{1}$$

where s is the perturbation frequency and ΔI_1 to ΔI_N are the current increments at the connection branches. The stability is defined by the roots of the characteristic determinant of the above homogeneous system:

$$\det \{[Z_A(s)] + [Z_P(s)]\} = 0 \tag{2}$$

where the newly introduced matrix $[Z_A(s)]$ is clearly identified through comparison with (1).

Obviously, the passive linear matrix $[Z_P]$ cannot exhibit any RHS poles. On the other hand, and because the active blocks are stable under an OC termination, the impedances $Z_{A,k}(s)$, $k = 1$ to N, cannot exhibit any RHS poles either. This is because $Z_{A,k}(s)$ agrees with the voltage-to-current closed-loop transfer function obtained under the excitation ΔI_k. Thus, the determinant in (2) cannot exhibit any poles in the RHS. As a result, there will be no uncertainties associated with cancellations/quasi-cancellations of RHS zeroes and poles. Note that the stability analysis of the active blocks described with $Z_{A,k}(s)$ is carried out through pole-zero identification in internal nodes to guarantee that there are no hidden instabilities. In case the blocks are SC–stable, the characteristic determinant should be written as:

$$\det \left\{ \begin{bmatrix} Y_{A,1}(s) & 0 & \ldots & 0 \\ 0 & Y_{A,2}(s) & \cdots & 0 \\ \vdots & \vdots & \ddots & \vdots \\ 0 & 0 & \ldots & Y_{A,N}(s) \end{bmatrix} + \begin{bmatrix} Y_{P,11}(s) & \ldots & Y_{P,1N}(s) \\ \vdots & \vdots & \vdots \\ Y_{P,N1}(s) & \ldots & Y_{P,NN}(s) \end{bmatrix} \right\} = 0 \tag{3}$$

where $Y_{A,n}$, where $n = 1 \ldots N$, are the admittance functions of the SC–stable active blocks and $[Y_P(s)]$ is the admittance matrix describing the purely passive linear network (we assume that this matrix is defined). In the practical stability analysis s is replaced with $j\Omega$ in either (2) or (3). One should calculate the N-port total impedance or admittance matrix at the ports defined in the partition, which can be readily done in commercial software. Then, one should obtain the determinant $\det(j\Omega)$, with the frequency Ω going from DC to a very high value (ideally infinite), which will depend on the gain response of the active devices. The determinant can be analyzed through both the Nyquist criterion or pole-zero identification [15]–[19]. The Nyquist plot is obtained in just a single Ω sweep (from DC to the maximum frequency considered) by tracing the imaginary part of $\det(j\Omega)$versus the real part. However, the Nyquist plot can be intricate and does not provide the explicit values of the zeroes. In contrast, pole–zero identification [15]–[19] does provide the numerical values of these zeroes, but may require a partition of the frequency band into elementary bands to ensure a sufficient accuracy. All the analyses presented here will be based on pole-zero identification.

As an illustrative example, a non-Foster transmission line [37]–[39] will be considered [Fig. 2(a)]. This has been chosen because it is prone to instability [40]–[43] and may contain a high number of active devices. The non-Foster transmission line allows the control of the phase delay of guided-wave devices, mostly applied for squint-free beamforming of antenna arrays [37]–[39]. The line is periodically loaded with negative capacitors implemented with transistor-based negative impedance converters (NICs) [Fig. 2(b)] [44]–[46]. Note that the aim of to use this line as a test-bench of the new analysis method. The design will be based on the one in [37], [38], where the NIC is implemented with two cross-coupled transistors having the capacitor to be negated, C_{neg}, connected between their emitter terminals, as shown in Fig. 2(b). This way an equivalent negative capacitor (ideally $-C_{neg}$) is obtained (in a certain bandwidth) when analyzing the input impedance between the terminal T_{C1} and ground. Note that a series resistor R, considered in Fig. 2(b), is often introduced to reduce the transconductance effects and facilitate a stable operation, as demonstrated in [45]. The group delay versus the excitation frequency is shown in Fig. 2(c) [37], [38].

Two relevant parameters affecting the stability properties are C_{neg} and the bias voltage V_{bb}. For an initial test, we have considered $V_{bb} = 0.85$ V, and varied C_{neg} in a wide range. The structure in Fig. 2(a) is partitioned taking into account that the NIC in Fig. 2(b) should be SC stable [45], [46]. This has been verified (considering full device models) through a stability analysis of the standalone NIC terminated in SC between T_{C1} and ground. Pole-zero identification has been applied (in a conventional manner) to a closed-loop transfer function. This is calculated inside the SC-terminated NIC, introducing a test current I in parallel at a node and obtaining the ratio between the node voltage and the test current $Z = V/I$ [see Fig. 2(b)].

Fig. 3(a) presents the variation of the real part of the dominant poles versus C_{neg} when the test current is introduced at the collector node of one of the two transistors. Because of the small size of the block, the same result is obtained at other nodes. As gathered from Fig. 3(a), this loaded NIC is SC-stable for all the C_{neg} values. Thus, the stability analysis of the entire structure will be based on the calculation of the determinant (3), where $Y_{A,n}$ is the input admittance of the NICs [Fig. 2(a)].

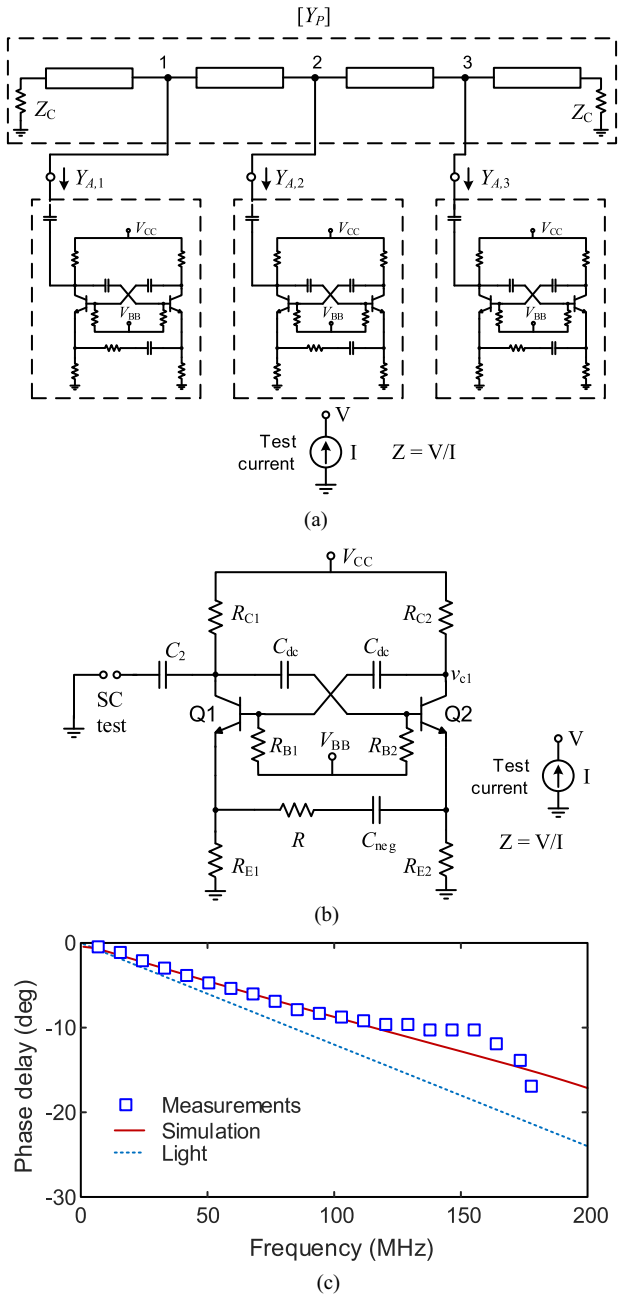

FIGURE 2. **Non-foster transmission line, as proposed in [37], [38]. (a) Schematic with $N = 3$ cells. (b) SC-stable NIC. (c) Variation of the phase delay versus frequency, with measurement points [37], [38].**

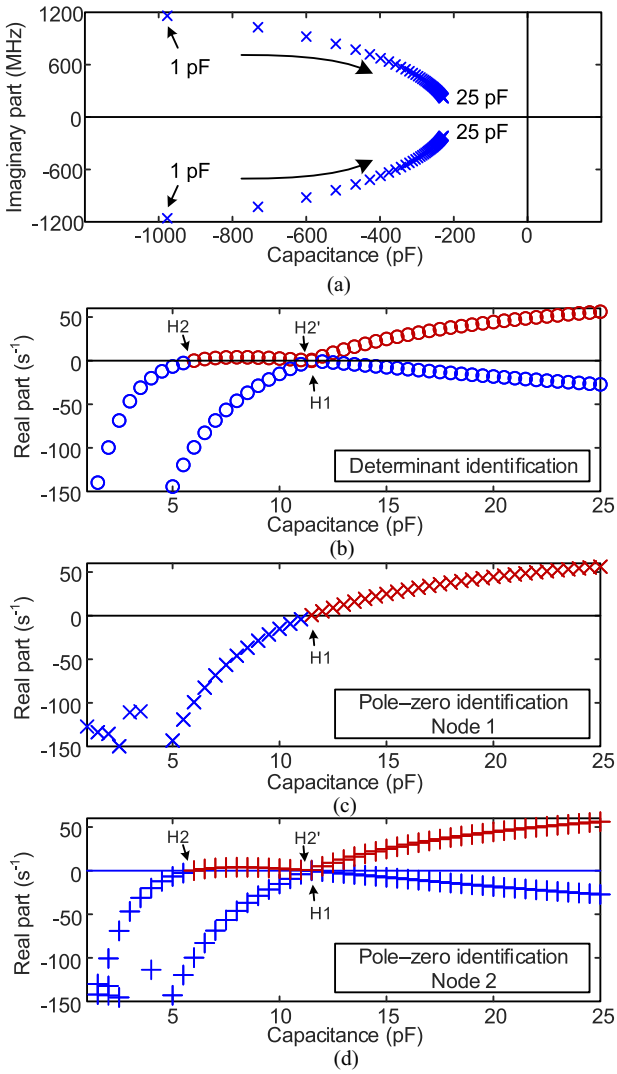

FIGURE 3. **Non-foster transmission line with $N = 3$ cells. (a) SC-stability analysis of the terminated NIC through conventional pole-zero identification applied to a closed-loop transfer function. The stability information is in the poles, traced with "x". (b) Stability analysis of the transmission line versus C_{neg} for $V_{bb} = 0.85$ V through the identification of the characteristic determinant in (3). The stability information is in the zeroes, traced with "o". (c) The same analysis through conventional pole-zero identification of a closed-loop transfer function at Node 1. The stability information is in the poles, traced with "x". (d) At Node 2.**

The results obtained when identifying the characteristic determinant of a transmission line containing $N = 3$ NIC stages are shown in Fig. 3(b). Note that now the stability information is in the zeroes. For the bias voltage $V_{bb} = 0.85$ V, there are two distinct pairs of complex-conjugate zeroes crossing to the RHS at $C_{neg} = 5.99$ pF and $C_{neg} = 11.43$ pF, respectively. The first pair of zeroes returns to the LHS at $C_{neg} = 11.43$ pF. This result will be compared with the one obtained with conventional pole-zero identification, applied to a closed-loop transfer function. Fig. 3(c) presents the variation of the real part of the dominant poles when this function is calculated at Node 1. The analysis is not able to predict the first crossing to the RHS, which delimits the stable C_{neg} interval. When calculating the closed-loop transfer function at Node 2 [Fig. 3(d)], the results are coincident with those obtained with the characteristic determinant.

The newly defined determinant accounts for the whole structure without any uncertainties associated with the cancellation/near cancellation of RHS zeroes and poles. Note, however, that the conventional pole-zero identification (applied to a closed-loop transfer function) [15]–[19] is used to verify the stability of the blocks considered in the partition. Moreover,

the identification of the determinant is based on the rigorous procedures developed in [15]–[19].

B. STABILITY BOUNDARIES

A bifurcation is a qualitative change of the solution stability properties when a parameter η is varied continuously [47], [48]. The most common one from a DC solution is the Hopf bifurcation, at which a pair of complex-conjugate poles $\sigma \pm j\Omega$ cross the imaginary axis at η_H. This will give rise to the onset/extinction of an oscillation at Ω with amplitude tending to zero [1], [3]. All the previous works [4]–[6] on bifurcation detection (in combination with commercial HB) rely on the calculation of the total admittance Y (in small-signal conditions) at an observation node. To obtain the bifurcation points, both Ω and η are optimized to fulfill $Y(\Omega,\eta_H) = 0$. Because the admittance is calculated in small signal, the η_H value(s) fulfilling $Y(\Omega,\eta_H) = 0$ will be the at the edge(s) of the oscillation interval, thus providing the stability limit. However, in a manner like pole-zero identification, this method may suffer from insufficient observability in large structures. To overcome this limitation, the bifurcation detection method presented here relies on the use (for the first time) of the characteristic determinant defined in the Section A.

At the Hopf bifurcation, the determinant (2) (or its alternative admittance version) will exhibit roots at $s = \pm j\Omega$, as corresponds to a pair of complex-conjugate poles crossing through the imaginary axis. Thus, the parameter value(s) at which the Hopf bifurcations take place is calculated replacing $s = j\Omega$ into (2) and solving the following complex equation for Ω and η_H:

$$\det\left[Z_T(\Omega,\eta_H)\right] = \det\left\{\begin{bmatrix} Z_{A,1}(j\Omega) & 0 & \dots & 0 \\ 0 & Z_{A,2}(j\Omega) & \cdots & 0 \\ \vdots & \vdots & \ddots & \vdots \\ 0 & 0 & \dots & Z_{A,N}(j\Omega) \end{bmatrix} + \begin{bmatrix} Z_{P,11}(j\Omega) & \dots & Z_{P,1N}(j\Omega) \\ \vdots & \vdots & \vdots \\ Z_{P,N1}(j\Omega) & \dots & Z_{P,NN}(j\Omega) \end{bmatrix}\right\} = 0 \quad (4)$$

Note that Ω is always an unknown, since the generated oscillation is autonomous and, thus, its frequency (even for amplitude tending to zero) varies with the parameter. In most cases one is interested on obtaining the stability boundaries in terms of two parameters η_1 and η_2. This is done by sweeping one of the parameters (η_1) and solving the bifurcation condition in terms of Ω and the other parameter (η_2). Prior to the works [24], [49]–[52], this was done through continuation methods [53], which use the solution point n as initial guess for the point $n+1$, as well as parameter switching [3] to circumvent the possible turning points. However, these methods are inherently local and will not be able to provide boundaries composed by several disconnected curves. In [24], [49]–[52], this problem has been addressed using contour-intersection methods, applied so far to obtain the zeroes of $Y(\Omega,\eta_1,\eta_2)$.

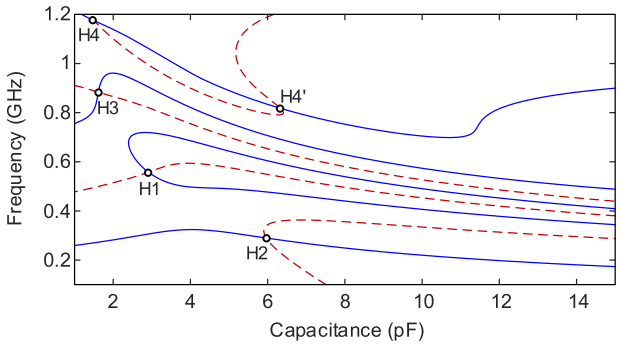

FIGURE 4. Contours $\det_r[Z_T(\Omega,\eta_2)] = 0$(blue solid line) and $\det_i[Z_T(\Omega,\eta_2)] = 0$(red dashed line) obtained for $N = 5$ cells and $\eta_1 = V_{bb} = 0.925$ V, traced in the plane defined by $\eta_2 = C_{neg}$ and Ω. There are five intersection points, corresponding to four disconnected Hopf-locus curves [see Fig. 5(b)].

However, the use of an admittance function calculated at a particular location may suffer from insufficient observability in complex structures.

Here the contour-intersection method will be applied for the first time to the characteristic determinant calculated as shown in Section II. For each η_1, a double sweep is carried out in Ω and η_2, which provides the functions $\det_r[Z_T(\Omega,\eta_2)]$ and $\det_i[Z_T(\Omega,\eta_2)]$, where the subscripts indicate real and imaginary parts, respectively. The above two functions constitute surfaces in their respective spaces $\Omega, \eta_2, \det_r$and $\Omega, \eta_2, \det_i$. Their respective intersections with the planes of zero value yield the two following contours:

$$\det_r\left[Z_T(\Omega,\eta_2)\right] = 0;\ \det_i\left[Z_T(\Omega,\eta_2)\right] = 0 \quad (5)$$

Finally, the intersections between the contours in (5) provide all the distinct bifurcation points, in terms of Ω and η_2, coexisting for each value of η_1.

The above method will be applied to obtain the Hopf-bifurcation boundaries in the case of the non-Foster transmission line of Fig. 2. Note that this is the first time that these stability boundaries are obtained using the purely numerical characteristic determinant defined in Section II. The previous work [22] described the structure in terms of a numerical matrix and an analytical matrix, the latter depending on the load elements C_{neg} and R, which, together with Ω, were unknowns of the complex equation $\det = 0$ for each value of η_1. As a result, it was virtually impossible to obtain the bifurcation locus in terms of η_1 and a second additional arbitrary parameter η_2. Moreover, the method did not allow numerical descriptions of the load elements, as might be required when considering parasitic effects.

The parameters considered in the new procedure are $\eta_1 = V_{bb}$ and $\eta_2 = C_{neg}$. To illustrate the procedure, Fig. 4 presents the contours $\det_r[Z_T(\Omega,\eta_2)] = 0, \det_i[Z_T(\Omega,\eta_2)] = 0$ for $\eta_1 = V_{bb} = 0.925$ V and $N = 5$ cells. They are traced in the plane defined by $\eta_2 = C_{neg}$ and the frequency Ω. As explained, all the Hopf bifurcations occurring (for a particular η_1) in terms of η_2, contained in the

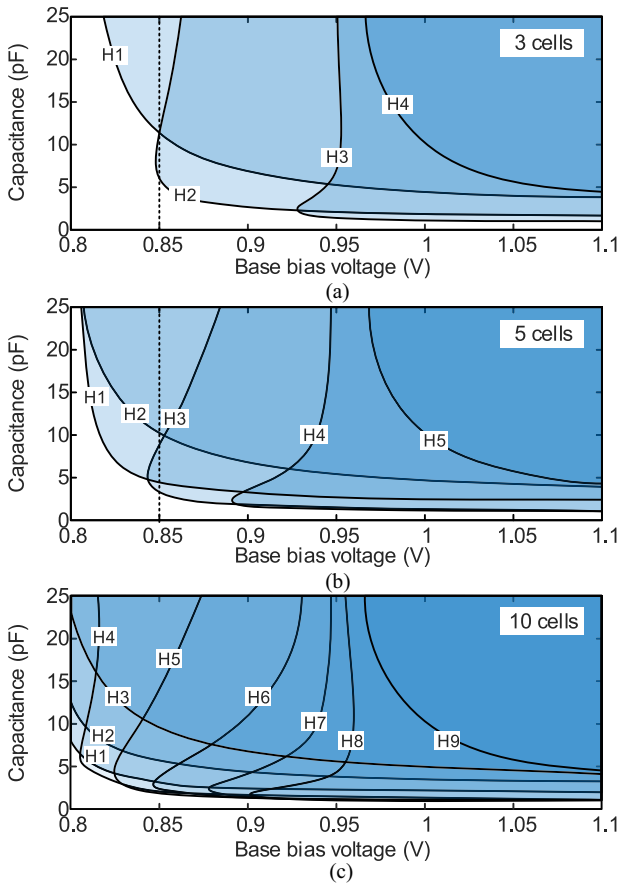

FIGURE 5. Non-Foster transmission line. Bifurcation loci in the plane defined by V_{bb} and C_{neg} for different numbers of cells. The white region corresponds to stable behavior. (a) $N = 3$ cells. (b) 5 cells. (c) 10 cells.

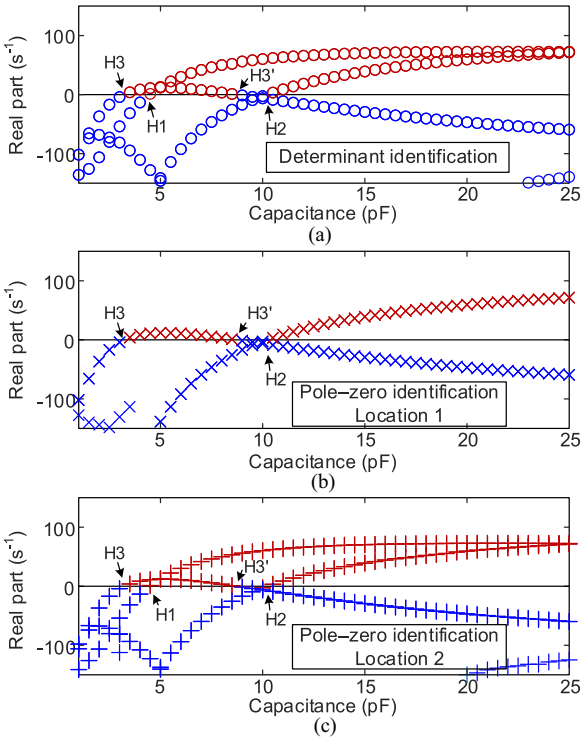

FIGURE 6. Validation of the stability predictions of the bifurcation loci in Fig. 5(b), with $N = 5$ cells, through a stability analysis versus C_{neg}, at constant $V_{bb} = 0.85$ V. (a) Pole-zero identification of the newly defined characteristic determinant. The stability information is in the zeroes, traced with "o". (b) Conventional pole-zero identification of a closed-loop transfer function calculated at Node 1. The stability information is in the poles, traced with "x". (c) The same at Node 2.

exploration intervals (of η_2 and Ω), are given by the intersections between the two contours. For $\eta_1 = V_{bb} = 0.925$ V there are five intersection points belonging to four disconnected Hopf-locus curves shown in Fig. 5(b). In fact, Fig. 5 presents the Hopf bifurcation loci for different numbers of cells. These Hopf loci are simultaneously obtained by sweeping η_1 and representing, at each sweep step, the intersection points in the plane defined by $\eta_1 = V_{bb}$ and $\eta_2 = C_{neg}$, with Ω as an implicit variable. See the correspondence between the intersection points obtained for $V_{bb} = 0.925$ V in Fig. 4 and the loci points at this V_{bb} value in Fig. 5(b), for $N = 5$ cells.

As gathered from Fig. 5, the Hopf bifurcations give rise to several disconnected curves, whose number increases with the number of stages. The stable region, in white color, decreases with N. For $N = 3$ stages, the loci predictions at $V_{bb} = 0.85$ V are in full agreement with those obtained through the identification of the characteristic determinant in Fig. 3(b) and conventional pole-zero identification applied to a closed-loop transfer function at Node 2 in Fig. 3(d). For $N = 5$ stages the identification of the determinant at $V_{bb} = 0.85$ V provides the results in Fig. 6(a). Again, the results obtained with conventional pole-zero identification depend on the location at which the closed-loop transfer function is calculated [see Fig. 6(b) and Fig. 6(c)]. At Node 2, these results agree with those obtained through the identification of the characteristic determinant. Finally, Fig. 7 presents an experimental validation of the stability boundaries for $N = 3$ stages, considering two V_{bb} values before and after crossing this boundary at $C_{neg} = 5.6$ pF.

In [23] the stability analysis in Section A was extended to large-signal operation and applied to a system of three Class-E amplifiers subject to coupling at their output ports, as may happen due to antenna cross talk. The large-signal analysis is carried out through a linearization of the HB equations about the periodic steady-state solution at ω_o with NH harmonic terms. The blocks considered in the partition must be stable under OC or SC terminations at the sideband frequencies $k\omega_o \pm \Omega$ arising under a small perturbation at Ω, which must be verified without affecting the steady-state solution at $k\omega_o$. Both this stability verification (based on conventional pole-zero identification) and the calculation of the characteristic determinant are carried out with the conversion-matrix approach [1], [3]. The implementation on commercial software is more demanding than in the small-signal case. As explained in [23], the verification of the SC/OC stability of the blocks is carried out with the aid of ideal filters, plus conventional pole-zero identification inside the blocks. On the other hand, the user

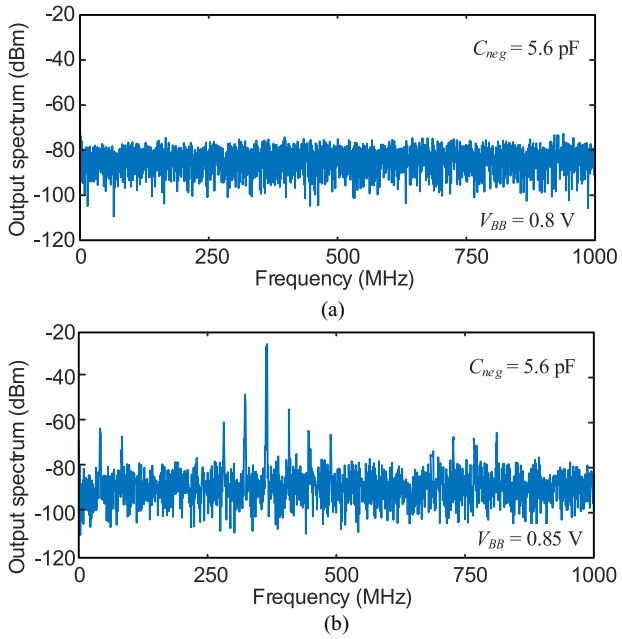

FIGURE 7. Experimental validation of the stability boundaries in the case of $N = 3$ stages for $C_{neg} = 5.6$ pF. (a) $V_{bb} = 0.8$ V. (b) $V_{bb} = 0.85$ V.

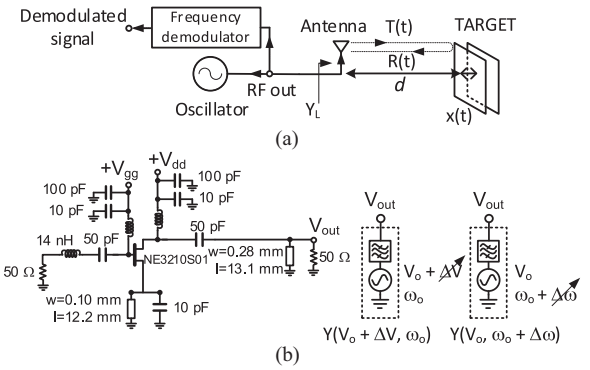

FIGURE 8. Doppler-radar system for the detection of vital signs using a self-injection locked oscillator, as proposed in [25], [33]–[35]. (a) Operation with a single antenna. (b) Standalone oscillator circuit. Extraction of the oscillator model from HB by applying finite differences to an auxiliary generator optimized to fulfill $Y(V_o, \omega_o) = 0$.

calculation of the conversion matrix at the partition ports requires the sequential introduction of a small-signal excitation source at each port and sideband frequency, in the presence of the ideal filters. The templates and a detailed description are provided in [23].

The new methodologies can be of interest for the stability analysis of any system containing multiple active devices and under the risk of exhibiting several unstable loops.

III. SEMI-ANALYTICAL FORMULATIONS FOR OSCILLATOR-BASED SYSTEMS

The HB analysis of free-running oscillations is generally carried out with various kinds of probes that prevent the undesired HB convergence towards the default non-oscillatory solution [1], [3], [54]. However, this circuit-level analysis may become demanding when the oscillator interacts with other elements. This section presents a semi-analytical formulation of this interaction, compatible with the use of commercial HB. In this formulation [24], [25], [36], the oscillator is represented with a realistic numerical model, extracted from HB and introduced into an analytical description of the complete system. This has two advantages: it avoids the convergence problems often encountered in HB and provides insight into the dependence of the oscillator solution on the external elements and parameters.

As an example, this section presents a general analysis of self-injection locked oscillators. This is the operation mode of the Doppler radar proposed in [33]–[35] for the detection of vital signs. For the first time we will present a stability analysis based on a semi-analytical formulation that considers the effect of the propagation delay on the signal envelope. Self-injection locking can also be used to reduce the phase noise of an existing oscillator through its connection to a delay line [55], [56] or a slow-wave structure [57], [58]. Here a method to reduce the phase-noise spectral density with minimum impact on the original oscillation frequency will be described for the first time.

A. SELF-INJECTION LOCKED OSCILLATOR

The total admittance function of a free-running oscillator is equal to zero at all its nodes [7], and, in particular, at its output node, the one connected to an antenna or to any external element. Thus, the oscillator in standalone conditions fulfills: $Y(V_o, \omega_o) = 0$ at this output node, where V_o and ω_o are the steady-state amplitude and frequency. Under self-injection conditions [Fig. 8(a)], there will be a variation of the equivalent output load. Its increment with respect to the original value Y_o (usually $Y_o = 0.02\ \Omega^{-1}$) will be $Y_L - Y_o = y_l(\omega, \bar{\mu})$, where $\bar{\mu}$ is a set of external parameters. In most cases, the self-injection will only give rise to small amplitude and frequency variations of the oscillation signal, so it will be possible to linearize the admittance function Y about the free funning point. Thus, under self-injection conditions one can write:

$$Y_T(V, \omega) \cong Y_V(V - V_o) + Y_\omega(\omega - \omega_o) + y_l(\omega, \bar{\mu}) = 0 \quad (6)$$

where Y_V and Y_ω are the amplitude and frequency derivatives of the oscillator admittance, calculated in standalone operation at V_o, ω_o. Note that $y_l(\omega, \bar{\mu})$ is not linearized due to the pronounced frequency variations often exhibited by this equivalent load under relevant delay effects. The derivatives Y_V and Y_ω can be obtained through finite differences by analyzing the *standalone* oscillator with an auxiliary generator (AG), introduced in commercial HB [4], [5]. The AG is a voltage source with amplitude V_o at the frequency ω_o in series with a bandpass filter at the same frequency [Fig. 8(b)]. It is optimized to fulfill the steady-state oscillation condition, given by the zero value of its current-to-voltage ratio: $Y(V_o, \omega_o) = 0$. This constitutes an outer-tier equation, whereas the pure HB system (with all the harmonic content)

constitutes the inner tier [3]. Then the derivative Y_V is calculated by setting the AG frequency to the steady-state value ω_o and performing a small sweep in V, as shown in Fig. 8(b). An analogous procedure is applied to calculate Y_ω. Splitting (6) into real and imaginary parts yields:

$$\begin{aligned} Y_{V,r}\,(V - V_o) + Y_{\omega,r}\,(\omega - \omega_o) + y_{l,r}(\omega, \bar{\mu}) = 0 \\ Y_{V,i}\,(V - V_o) + Y_{\omega,i}\,(\omega - \omega_o) + y_{l,i}(\omega, \bar{\mu}) = 0 \end{aligned} \tag{7}$$

Eliminating $(V - V_o)$ one obtains a scalar equation in ω:

$$\omega = \omega_o - \frac{Y_{V,r}}{\det_o} y_{l,i}(\omega, \bar{\mu}) + \frac{Y_{V,i}}{\det_o} y_{l,r}(\omega, \bar{\mu}) \tag{8}$$

where $\det_o = Y_{V,r}Y_{\omega,i} - Y_{V,i}Y_{\omega,r}$. To obtain the solution curve in terms of a given parameter μ_i contained in $\bar{\mu}$, one may perform a double sweep in μ_i and ω, and calculate the zero-value contour [59] of the scalar function:

$$H(\omega, \mu_i) = \omega - \omega_o + \frac{Y_{V,r}}{\det_o} y_{l,i}(\omega, \mu_i) - \frac{Y_{V,i}}{\det_o} y_{l,r}(\omega, \mu_i) \tag{9}$$

The contour $H(\omega, \mu_i) = 0$ provides the function $\omega(\mu_i)$. Once the frequency is known, the oscillator output amplitude is directly calculated replacing $\omega(\mu_i)$ in (12).

The formulation (11)-(12) can be applied to obtain the solution curves of a self-injection locked radar [33]–[35] versus the distance to the target d [Fig. 8(a)]. Note that the frequency modulation due to the target movement is analyzed in Section D. The oscillator signal is transmitted by the antenna, reflected by the target at the distance d, and received back by the antenna, with a certain attenuation and phase shift. In fact, the reflection coefficient for transmit and receive antenna gain G_t and G_r and distance to the target d [Fig. 1(b)] is expressed as [60]:

$$\Gamma(G, d, \omega) = \sqrt{\frac{G_t G_r \sigma \lambda^2}{(4\pi)^3 d^4}} e^{-j\omega\frac{2d}{c}} \tag{10}$$

where σ is the radar cross section and c is the speed of light. The corresponding admittance, looking into the antenna terminals, will be: $Y_L = Y_o(1-\Gamma)/(1+\Gamma)$. For the usual attenuation values, it will be possible to approach Y_L with its first-order Taylor expansion about $\Gamma = 0$, which provides: $Y_L = Y_o(1-2\Gamma)$. And the admittance increment y_l with respect to Y_o is:

$$y_l(\omega, \bar{\eta}) = -\frac{c}{\omega R_r d^2}\sqrt{\frac{G_{tot}\sigma}{4\pi}} e^{-j\frac{2d}{c}\omega} = -\frac{\eta\sqrt{G_{tot}}}{\omega d^2} e^{-j\frac{2d}{c}\omega} \tag{11}$$

where the parameter η has been introduced. In the case of a single antenna, one will have $\sqrt{G_{tot}} = G$. Replacing (14) into (11), one obtains the following relationship:

$$H(\omega) = \omega - \omega_o - \frac{|Y_V|}{\det_o}\frac{\eta G}{\omega d^2}\sin\left(\frac{2d\omega}{c} + \alpha_v\right) = 0 \tag{12}$$

As gathered from (15), the distance values at which the oscillation frequency agrees with the free-running one are spaced in λ/4, that is, $d_{n+1} - d_n = \lambda/4$.

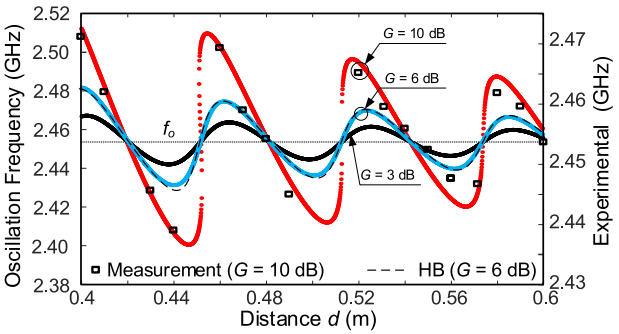

FIGURE 9. Self-injection locked radar. Variation of the oscillation frequency versus the distance *d* calculated with (8) for three antenna-gain values, *G* = 3.0 dB, *G* = 6 dB and *G* =10 dB. Full circuit-level HB simulations for G = 6 dB are superimposed. Measurements for *G* = 10 dB are shown.

As an application example, the Doppler radar for the detection of vital signs proposed in [33]–[35] has been considered. The system is sketched in Fig. 8. The oscillator is based on the FET NE3210S01 [25] and built on Rogers 4003C substrate [Fig. 8(b)]. The considered radar cross section is $\sigma = 0.5$ m^2. Fig. 9 presents the variation of the oscillation frequency versus the distance d for three antenna-gain values, $G = 3.0$ dB, $G =$ 6 dB and $G =$10 dB. Full circuit-level HB simulations for G = 6 dB are superimposed. The excellent agreement confirms the validity of the linearization of $Y(V,\omega)$, as well as the whole semi-analytical formulation (7). As gathered from the figure, the frequency excursion is larger when increasing the antenna gain, which will enable a higher sensitivity to the instantaneous target movement (see the slope at the free-running frequency). However, when increasing the gain, the solution curve becomes multi-valued in a small d interval (for $G = 10$ dB), with no HB convergence, and undesired physical jumps between distinct curve sections. For all the gain values, the oscillation frequency agrees with the free-running one when $\sin(2d\omega/c + \alpha_v) = 0$.

B. STABILITY ANALYSIS

The following stability analysis of self-injection locked oscillators will consider the time delay of the signal envelope. The load admittance will be expressed as:

$$y_l(\omega, \bar{\mu}) = -F(\omega, \bar{\mu})e^{-j\omega\tau} \tag{13}$$

where τ is the time delay. For the stability analysis of a given steady state solution (V, ω), a small-amplitude perturbation will be introduced in system (6), so the oscillator amplitude and phase become $V + \delta v(t)$ and $\delta\phi(t)$, respectively. Then, the phasor of the perturbed solution can be expressed as $X(t) = V + \delta X(t)$, where $\delta X(t) = jV\delta\phi(t) + \delta V(t)$. The frequency domain equation corresponding to the phasor $X(\Omega)$ is given by:

$$\begin{aligned} &\big(Y\,(V + \delta V(\Omega), \omega + \Omega) \\ &\quad - F(\omega + \Omega, \bar{\mu})e^{-j(\omega+\Omega)\tau}\big)\,X(\Omega) = 0 \end{aligned} \tag{14}$$

where $Y(V,\omega) \equiv Y_V(V - V_o) + Y_\omega(\omega - \omega_o)$ and $X(\Omega) = V\delta(0) + \delta X(\Omega)$. Now, equation (14) will be translated to the envelope domain by applying the inverse Fourier transform and neglecting second order terms in the perturbation components:

$$\begin{aligned} &Y(jV\delta\phi + \delta V) + Y_V V\delta V - jY_\omega(jV\delta\dot{\phi} + \delta\dot{V}) \\ &\quad + y_l(\omega,\bar{\mu})(jV\delta\phi_d + \delta V_d) \\ &\quad + jF_\omega(\omega,\bar{\mu})e^{-j\omega\tau}(jV\delta\dot{\phi}_d + \delta\dot{V}_d) = 0 \end{aligned} \tag{15}$$

where $Y \equiv Y(V,\omega)$ and the time-delayed terms $\delta\phi_d \equiv \delta\phi(t-\tau)$ and $\delta V_d = \delta V(t-\tau)$ arise naturally when applying the inverse Fourier transform $\Im^{-1}\{e^{-j\Omega\tau}X(\Omega)\} = X(t-\tau)$. Note that a first-order Taylor-series expansion has been carried out in the amplitude term $F(\omega+\Omega)$, with less pronounced frequency variation than the complex exponential $e^{-j\omega\tau}$. Now, to obtain the poles of linear system (15), the perturbation components will be expressed as $\delta V = U_V e^{st}$ and $\delta\phi = U_\phi e^{st}$, yielding:

$$\begin{aligned} &\big(Y + y_l(\omega,\bar{\mu})e^{-s\tau} + Y_V V \; -j(Y_\omega - F_\omega(\omega,\bar{\mu})e^{-j\tau(\omega+s)})s\big) \\ &U_V + \big(jY + jy_l(\omega,\bar{\mu})e^{-s\tau} \\ &\quad +(Y_\omega - F_\omega(\omega,\bar{\mu})e^{-j\tau(\omega+s)})s\big)\,U_\phi = 0 \end{aligned} \tag{16}$$

Splitting (16) into real and imaginary parts, an homogeneous equation $A(s,\tau)\bar{U} = \bar{0}$ is obtained, where $\bar{U} = [U_V U_\phi]^t$. Then, in a manner like the analysis in Section II, the stability properties are defined by the zeroes $s = \lambda(\tau)$ of the characteristic determinant $\det A(s,\tau)$. Note that expanding the term $e^{-s\tau}$ in (16) in a power series produces $p(s,\tau) = O(s)$, since the steady state terms cancel each other as $Y + y_l(\omega,\bar{\mu}) = 0$. Then, one of the zeroes is $\lambda(\tau) = 0$ as expected due to the system autonomy. For convenience, this root can be removed from the characteristic determinant considering $\det A(s,\tau)/s$.

The above analysis has been applied to the self-injection locked radar considered in Fig. 8, with the time delay is $\tau = 2d/c$. The antenna gain is $G = 10$ dB. The dominant poles have been calculated identifying the function $\det A(s,\tau)/s$, in a manner like what was done in Section II. The identification has been carried out in Matlab R2021a, using the System Identification toolbox. This requires the preselection of the identification order, which has been set to $n = 20$ to get a percent fit to estimation data greater than 99.03% for all distance values. Fig. 10(a) presents the variation of the real part of the dominant roots of $\det A(s,\tau)/s$ versus d. For most of the d values there is a dominant real root that crosses from the LHS to the RHS at $d = 0.451$ m and then back to the LHS at $d = 0.4511$ m. The crossing of a real root through zero gives rise to a singularity of the Jacobian matrix of the steady-state system, so the solution curve exhibits an infinite slope at these crossing points, also known as *turning points*. For $G = 10$ dB in Fig. 10, the solution is unstable in the small d interval comprised between the two turning points. Although the unstable interval is small, there will be an undesired discontinuous jump when reaching any of the two turning points (when either increasing or decreasing d).

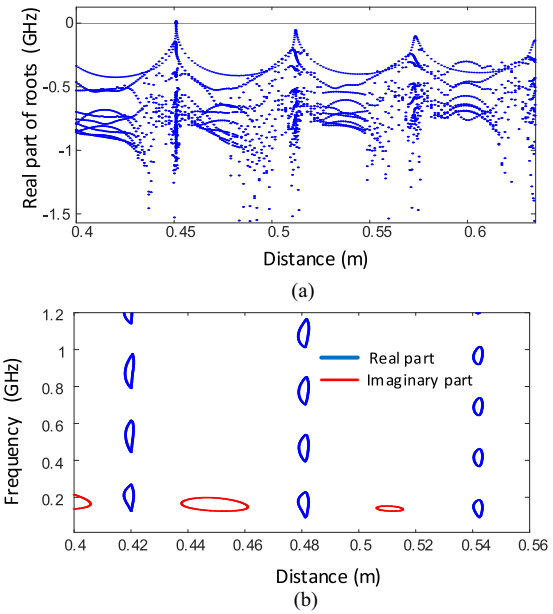

FIGURE 10. Self-injection locked radar. (a) Stability analysis versus the distance d. For most of the d values there is a dominant real root and several additional real and complex roots, resulting from the delay effect. (b) Detection of the possible Hopf bifurcations. Contours of the real and imaginary parts of $\det A(j\Omega,\tau)/j\Omega$, traced in the plane defined by d and Ω. There are no intersections for $d > 0.4$ m, so no Hopf bifurcations are obtained in this distance range for $G = 10$ dB (or smaller values).

As in Section II, possible Hopf bifurcations would fulfill $\det A(j\Omega,\tau)/j\Omega = 0$. Fig. 10(b) presents the contours of the real and imaginary parts of $\det A(j\Omega,\tau)/j\Omega = 0$ in the plane defined by d and Ω. As can be seen there are no intersections for $d > 0.4$ m, so no Hopf bifurcations are obtained in this distance range for $G = 10$ dB (or smaller values). Note that the Hopf bifurcations would require significant delay effects for the exponential $e^{-s\tau}$ to have an impact on the stability properties. This implies large d values at which the self-injection signal is too attenuated to cause incommensurate oscillations. However, it is interesting to note how the contours of the real and imaginary parts of the function $\det A(j\Omega,\tau)/j\Omega = 0$ [Fig. 10(b)] are closer for smaller d.

C. ANALYSIS UNDER MODULATED CONDITIONS

The target movement will give rise to a time-varying distance $2d + 2x(t)$ where $x(t) << d$ that will produce a modulation of the oscillation amplitude and frequency (V,ω). Under this modulation, the oscillator solution can be expressed as:

$$X(t) = (V + \delta V(t))e^{j\int\delta\omega(t)dt} = V(t)e^{j\delta\phi(t)} \tag{17}$$

where $\delta\omega(t) = \omega(t) - \omega$ and $X(t)$ is the time-varying amplitude. The dynamics of the components of $X(t)$ are governed by equation (15). Since $\dot{x}(t) \ll c$, the time variation of the

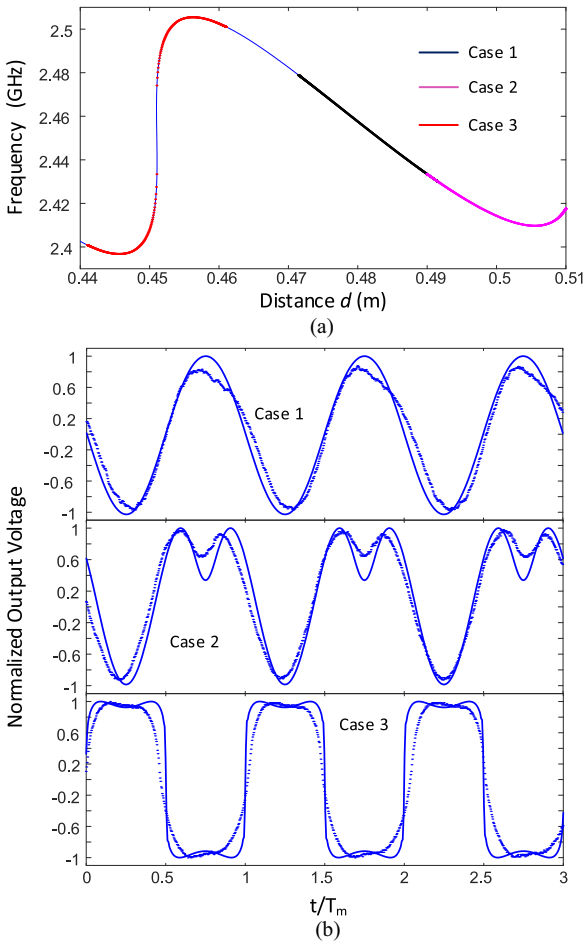

FIGURE 11. Analysis under modulated conditions with $G = 10$ dB. Three different operation points have been considered: $d = 0.4815$ m (Case 1), corresponding to the original free-running frequency, $d = 0.5$ m (Case 2) and $d = 0.451$ m (Case 3), between the two turning points. (a) Modulated frequency versus the time varying distance projected over the $\omega(d)$ curve. (b) Waveforms demodulated using a frequency discriminator. Time is normalized to the modulation period T_m. The theoretical (solid line) and experimental (dotted line) signals are compared.

phasor $X(t)$ is too slow to be affected by the time delay $\tau = (2d + x(t))/c$, so one can approach $X(t-\tau) \simeq X(t)$. On the other hand, through the inspection of Fig. 10(a), we will choose a stable operation point with dominant zeroes that, in comparison with other points, are far from the imaginary axis. The aim is to have a negligible effect of the circuit natural frequencies. Consequently, the modulated signal varies slowly in comparison with the time constants of the perturbed system. Under these circumstances, the modulated solution $(V(t), \omega(t))$ can be obtained from the quasi-static equation:

$$Y\left(V(t), \omega(t)\right) - F(\omega(t), \bar{\mu}) \exp\left(-j\omega(t)\frac{2(d+x(t))}{c}\right) = 0 \qquad (18)$$

This equation has been applied to calculate the modulated solution resulting from the periodic motion of metal plate with an amplitude excursion of 1 cm at the frequency 2.7 Hz, which has been implemented in the experiment using a motor. As shown in Fig. 8(a), the modulation signal is extracted with a phase discriminator that includes an amplifier. A gain $G = 10$ dB and three different (central) distance values have been considered: $d = 0.4815$ m (Case 1), corresponding to the original free-running frequency, $d = 0.5$ m (Case 2) and $d = 0.451$ m (Case 3), between the two turning points.

In Fig. 11(a) the modulated frequency is traced versus the time-varying distance in the three cases, showing the respective excursions along the oscillation-frequency curve versus the distance d. Fig. 11(b) compares the demodulated theoretical and experimental waveforms. Case 1 provides a sinusoidal signal; Case 2 gives rise to some distortion and Case 3 provides a near-square output voltage in consistency with the infinite-slope points in static conditions. Very good agreement between simulation and measurements is obtained in the three cases.

D. PHASE-NOISE REDUCTION WITH A SLOW-WAVE STRUCTURE

To get insight into the phase noise of a self-injection locked system, we will perform this noise analysis assuming a single dominant real pole, which will be valid in most of the stable operation regions [Fig. 10(a)]. The analysis under a single real pole is carried out approaching $F(j\omega + s)e^{-j(\omega+s)\tau} \cong F(j\omega)e^{-j\omega\tau} - jy_{l\omega}(j\omega)s$, where $y_{l\omega}$ is the frequency derivative of y_l. Under this approach and in the presence of an equivalent noise current $i_n(t)$ at the analysis node, one obtains the perturbation equation:

$$Y_V \delta v(t) + (Y_\omega + y_{l\omega})\left(-\frac{j\delta\dot{v}(t)}{V_o} + \delta\dot{\phi}(t)\right) = \frac{i_n(t)}{V_o} \qquad (19)$$

Note that the term on the left-hand side is directly derived from (15) when applying the mentioned approach. The phase noise spectrum is obtained [7] by (i) splitting (16) into real and imaginary parts, (ii) applying the Fourier transform, (iii) considering that the real and imaginary parts of the white-noise contribution are uncorrelated, and (iv) solving for $|\delta\phi(\Omega)|^2$:

$$|\delta\phi(\Omega)|^2 = \frac{\left(|Y_V|^2 + \frac{|Y_\omega + y_{l\omega}|^2}{V_o^2}\Omega^2\right) 2\frac{|I_n(\Omega)|^2}{V_o^2}}{\left[\det_o + Y_{V,r}y_{l\omega,i} - Y_{V,i}y_{l\omega,r}\right]^2\Omega^2 + \Omega^4\frac{|Y_\omega + y_{l\omega}|^4}{V_o^2}} \qquad (20)$$

where $\det_o = Y_{V,r}Y_{\omega,i} - Y_{V,i}Y_{\omega,r}$. The dominant real pole [4], [7] of a stable standalone oscillator is proportional is $-\det_o P$, where P is a positive quantity. Thus, we will have $\det_o > 0$. The equivalent noise current $i_n(t)$ is estimated with the oscillator in standalone free-running operation. Its value is fitted so that the phase-noise spectrum obtained with (20) in standalone conditions ($y_l = 0$) matches the one obtained with a circuit-level analysis, using the conversion-matrix approach [61], [62]. The upconverted flicker noise can be also considered when performing this fitting.

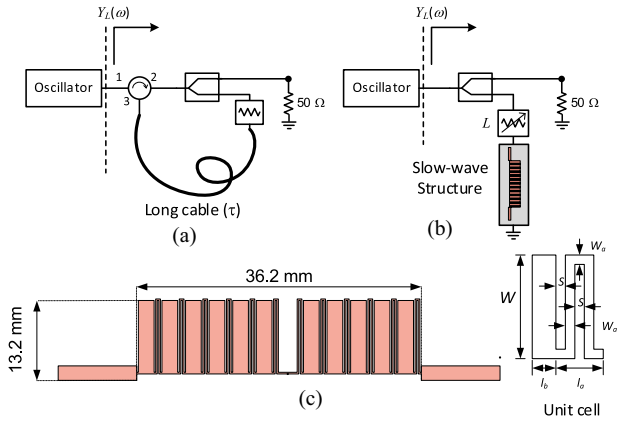

FIGURE 12. Self-injection locked oscillator for phase noise reduction. (a) Long cable considered in the theoretical analysis [55], [56]. (b) Slow-wave structure based on a unit cell made up of a Schiffman section and an open-ended stub [57].

Initially we will consider the case [54]–[55] of an oscillator loaded with a circulator having a long cable with the delay τ and an attenuator connected between the circulator ports 2 and 3 [Fig. 12(a)]. The admittance increment due to the pulling effects is:

$$y_l(\omega) = Y_o \frac{1-\Gamma(\omega)}{1+\Gamma(\omega)} - Y_o \cong [1-2\Gamma(\omega)]\, Y_o - Y_o = -2\rho e^{-j\omega\tau} Y_o \qquad (21)$$

where the approximation valid for relatively high attenuation effects (as expected in these applications) has been considered. Replacing this expression in (12), the oscillation frequency is:

$$H = \omega - \omega_o + \frac{2\rho Y_o}{\det_o} |Y_V| \sin(\omega\tau + \alpha_V) = 0 \qquad (22)$$

where α_V is the angle of Y_V. Thus, the oscillation frequency agrees with the free-running one at $\tau_n = (n\pi - \alpha_V)/\omega_o$, where n is an integer.

Replacing the frequency derivative of (21) in (20) and neglecting higher order terms in Ω one obtains:

$$|\delta\phi(\Omega)|^2 = \frac{2|Y_V|^2 \frac{|I_w(\Omega)|^2}{V_o^2}}{[\det_o + 2\rho(\tau) Y_o \tau\, |Y_V| \cos(\omega\tau + \alpha_V)]^2 \Omega^2} \qquad (23)$$

Local minima and maxima of the phase noise will be obtained when $\cos(\omega\tau_n + \alpha_V) = \pm 1$. The minima, corresponding to the positive sign, tend to be lower for higher τ. However, one must keep in mind that ρ decreases with τ. At the values of the local minima, denoted as τ_{2n}, the oscillation frequency agrees with the one obtained in standalone operation. In the absence of self-injection locking (τ) the phase noise in (23) agrees with the one obtained in free-running conditions, having the denominator $\det_o{}^2\Omega^2$. For a higher $\det_o{}^2$ (as obtained for a large quality factor of the standalone oscillator), a higher τ is required to obtain a significant phase noise reduction.

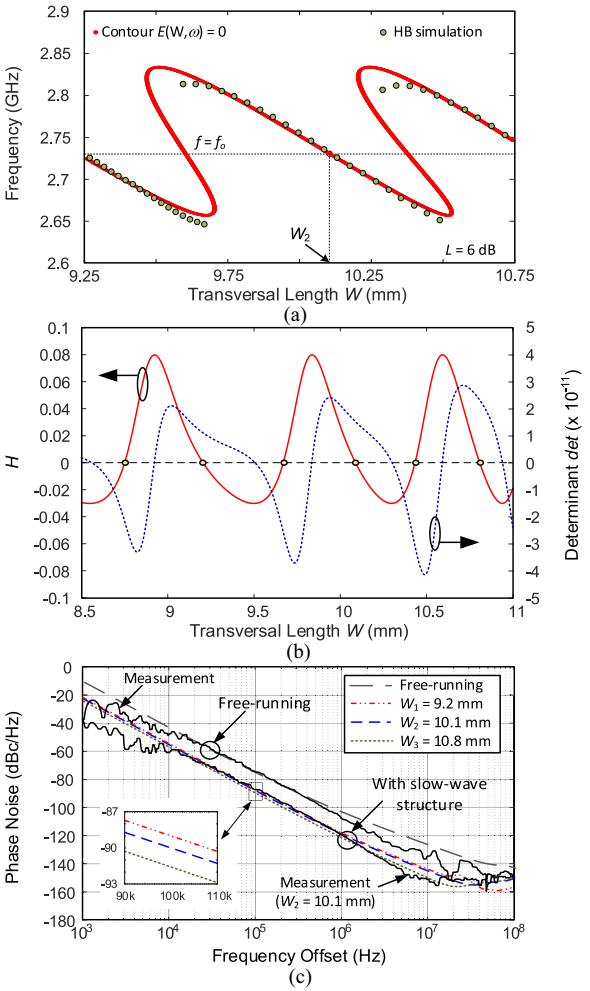

FIGURE 13. Phase-noise reduction using a slow-wave structure with a minimum impact on the original free-running frequency ω_o. (a) Variation of the oscillation frequency versus the transversal length W of the Schiffman section with measurements superimposed. (b) Variation of the error function H as well as the term det in (26) versus W. (c) Phase-noise spectra at three consecutive W values providing the oscillation frequency ω_o and high positive values of det.

For a compact implementation, one can use a slow-wave structure [57], [58] instead of a long cable. The configuration considered in this work is shown in Fig. 12(b). The oscillator is terminated with a load network that contains a slow-wave structure based on a unit cell made up of a Schiffman section [57] and an open-ended stub. The augmented oscillator is governed by the equations (7) and (8). The variation of the oscillation frequency versus the transversal length W is shown in Fig. 13(a), where experimental measurements are superimposed. As gathered from this figure, a possible drawback of the self-injection topology is the impact of the load network on the oscillation frequency, which may undergo an undesired shift from the standalone value ω_o. To have $\omega = \omega_o$, the following condition must be fulfilled:

$$Y_{V,r} y_{l,i}(\omega_o, \bar{\mu}) - Y_{V,i} y_{l,r}(\omega_o, \bar{\mu}) = 0 \qquad (24)$$

where y_l is the input admittance Y_L of the slow-wave structure (Fig. 12) minus Y_o. The amplitude increment is:

$$V - V_o = \frac{y_{l,r}(\omega_o, \bar{\mu})}{Y_{V,r}} = \frac{y_{l,i}(\omega_o, \bar{\mu})}{Y_{V,i}} \tag{25}$$

In general, due to the attenuation of the self-injection signal, the amplitude increment will be small. Nevertheless, this increment can be monitored using equation (25). If it is too large, the linearization will be invalid, and a different operation point must be chosen. To minimize the phase-noise spectral density at ω_o, one should maximize:

$$\begin{aligned} \det &= \det_o + Y_{V,r} y_{l\omega,i}(\mu, \omega_o) - Y_{V,i} y_{l\omega,r}(\mu, \omega_o) \\ &= \det_o + |Y_V|\,|y_{l\omega}| \sin\left(ang(y_{l\omega}) - \alpha_V\right) \end{aligned} \tag{26}$$

Improving the spectral purity of a lower phase-noise oscillator (with a high $\det_o$) is more demanding and will require a higher quality factor of the slow-wave structure.

Note that the derivative of the admittance increment $y_{l\omega}$ is evaluated at ω_o. The function (26), under the fulfilment of (24), can be maximized analyzing the slow-wave structure only. This is done by introducing the error function H in (22) as well as the determinant in (26) as user equations in the simulation of the passive linear slow-wave structure. Note that both depend on the constant values of the derivatives of the standalone oscillation Y_V and Y_ω, obtained at an earlier stage (when extracting the oscillator model from HB). More specifically, the simulation of the slow-wave structure provides $Y_L(\omega)$ from which the admittance increment is obtained as $y_l(\omega) = Y_L(\omega) - Y_o$. Then, the derivative $y_{l\omega}(\omega)$ is calculated with a simple frequency differentiation.

Fig. 13(b) shows the variation of the error function H as well as the term det in (26) versus the transversal length W of the slow-wave structure. The oscillation frequency of the augmented oscillator agrees with the free running one at the points where $H = 0$. To minimize the impact of the slow-wave structure on ω, one of these points should be selected. The magnitude of det increases with W, which should lead to a higher phase noise reduction. In agreement with the demonstration in (21)-(23), considering a simple delay line, the maxima, and minima of det alternate. As W increases, the extremes of det become closer to the W values yielding $\omega = \omega_o$. The phase-noise spectra obtained at three consecutive W, which provide $\omega = \omega_o$ and high positive values of det are shown in Fig. 13(c). As shown in the expanded view, the maximum phase-noise reduction is obtained for the higher transversal length $W = 10.8$ mm.

IV. CONCLUSION

Recent advances in stability analysis, at circuit level, and oscillator analysis, through semi-analytical formulations, have been presented. The stability analysis, intended for large circuits containing multiple devices, is based on a calculation of the characteristic determinant that, by construction, cannot exhibit any poles in the right-hand side of the complex plane. Then, a method to obtain the stability boundaries in multi-device circuits using the newly defined characteristic determinant has been presented for the first time. It has been illustrated through its application to a non-Foster transmission line considering up-to ten negative impedance converters. The semi-analytical formulations have been illustrated through their application to a self-injection locked radar, where the effect on the stability properties of the time delay in the signal envelope has been considered for the first time. Self-injection locked oscillators for phase-noise reduction have also been investigated, and a new semi-analytical method to reduce the impact of the self-injection loop on the original free-running oscillation frequency has been presented.

REFERENCES

[1] V. Rizzoli and A. Neri, "State of the art and present trends in nonlinear microwave CAD techniques," *IEEE Trans. Microw. Theory Techn.*, vol. 36, no. 2, pp. 343–365, Feb. 1988.

[2] K. S. Kundert, "Introduction to RF simulation and its application," *IEEE J. Solid-State Circuits*, vol. 34, no. 9, pp. 1298–1319, Sep. 1999.

[3] R. Quéré, A. Suarez, E. Ngoya, M. Hessane, J. Obregon, and M. Camiade, "Large signal design of broad-band monolithic microwave frequency dividers and phase-locked oscillators," *IEEE Trans. Microw. Theory Techn.*, vol. 41, no. 11, pp. 1928–1938, Nov. 1993.

[4] A. Suárez, *Analysis and Design of Autonomous Microwave Circuits*. Hoboken, NJ, USA: Wiley, 2008.

[5] A. Suárez and R. Quere, *Stability Analysis of Nonlinear Microwave Circuits*. Norwood, MA, USA: Artech House, 2002.

[6] S. Jeon, A. Suárez, and D. B. Rutledge, "Global stability analysis and stabilization of a class-E/F amplifier with a distributed active transformer," *IEEE Trans. Microw. Theory Techn.*, vol. 53, no. 12, pp. 3712–3722, Dec. 2005.

[7] K. Kurokawa, "Some basic characteristics of broadband negative resistance oscillator circuits," *Bell Syst. Techn. J.*, vol. 48, no. 6, pp. 1937–1955, 1969.

[8] V. Rizzoli and A. Lipparini, "General stability analysis of periodic steady-state regimes in nonlinear microwave circuits," *IEEE Trans. Microw. Theory Techn.*, vol. 33, no. 1, pp. 30–37, Jan. 1985.

[9] A. Platzker, W. Struble, and K. T. Hetzler, "Instabilities diagnosis and the role of k in microwave circuits," in *IEEE MTT-S Int. Microw. Symp. Dig.*, 1993, vol. 3, pp. 1185–1188.

[10] F. Bonani and M. Gilli, "Analysis of stability and bifurcations of limit cycles in Chua's circuit through the harmonic-balance approach," *IEEE Trans. Circuits Syst. I, Fundam. Theory Appl.*, vol. 46, no. 8, pp. 881–890, Aug. 1999.

[11] L. Pantoli, G. Leuzzi, A. Santarelli, and F. Filicori, "Stability analysis and design criteria of paralleled-device power amplifiers under large-signal regime," *IEEE Trans. Microw. Theory Techn.*, vol. 64, no. 5, pp. 1442–1455, May 2016.

[12] S. Colangeli, W. Ciccognani, and E. Limiti, "Algorithmic test of the unconditional stability of three-port networks," *IEEE Trans. Microw. Theory Techn.*, vol. 66, no. 12, pp. 5197–5205, Dec. 2018.

[13] A. Suárez, "Check the stability: Stability analysis methods for microwave circuits," *IEEE Microw. Mag.*, vol. 16, no. 5, pp. 69–90, Jun. 2015.

[14] W. Struble and A. Platzker, "A rigorous yet simple method for determining stability of linear N-port networks [and MMIC application]," in *Proc. 15th Annu. GaAs IC Symp.*, Oct. 1993, pp. 251–254.

[15] J. Jugo, J. Portilla, A. Anakabe, A. Suarez, and J. M. Collantes, "Closed-loop stability analysis of microwave amplifiers," *IEE Electron. Lett.*, vol. 37, pp. 226–228, 2001.

[16] A. Anakabe *et al.*, "Analysis and elimination of parametric oscillations in monolithic power amplifiers," in *Proc. IEEE MTT Symp.*, 2002, vol. 3, pp. 2181–2184, doi: 10.1109/MWSYM.2002.1012304.

[17] N. Ayllon, J.-M. Collantes, A. Anakabe, I. Lizarraga, G. Soubercaze-Pun, and S. Forestier, "Systematic approach to the stabilization of multitransistor circuits," *IEEE Trans. Microw. Theory Techn.*, vol. 59, no. 8, pp. 2073–2082, Aug. 2011.

[18] J. M. Collantes, I. Lizarraga, A. Anakabe, and J. Jugo, "Stability verification of microwave circuits through floquet multiplier analysis," in *Proc. IEEE Asia-Pacific Conf. Circuits Syst.*, 2004, vol. 2, pp. 997–1000.

[19] J.-M. Collantes *et al.*, "Pole-Zero identification: Unveiling the critical dynamics of microwave circuits beyond stability analysis," *IEEE Microw. Mag.*, vol. 20, no. 7, pp. 36–54, Jul. 2019.

[20] A. Cooman, F. Seyfert, M. Olivi, S. Chevillard, and L. Baratchart, "Model-free closed-loop stability analysis: A linear functional approach," *IEEE Trans. Microw. Theory Techn.*, vol. 66, no. 1, pp. 73–80, Jan. 2018.

[21] C. Barquincro, A. Suárez, A. Herrera, and J. L. García, "Complete stability analysis of multifunction MMIC circuits," *IEEE Trans. Microw. Theory Techn.*, vol. 55, no. 10, pp. 2024–2033, Oct. 2007.

[22] A. Suarez and F. Ramirez, "Stability and bifurcation analysis of multi-element non-Foster networks," *IEEE Trans. Microw. Theory Techn.*, vol. 66, no. 4, pp. 1817–1830, Apr. 2018.

[23] A. Suarez and F. Ramirez, "Two-level stability analysis of complex circuits," *IEEE Trans. Microw. Theory Techn.*, vol. 69, no. 1, pp. 132–146, Jan. 2021.

[24] A. Suarez, F. Ramirez, and R. Melville, "Nonlinear analysis of oscillator mutual injection locking through inductor coupling," *IEEE Trans. Microw. Theory Techn.*, vol. 69, no. 1, pp. 812–824, Jan. 2021.

[25] M. Ponton, A. Herrera, and A. Suarez, "Wireless-coupled oscillator systems with an injection-locking signal," *IEEE Trans. Microw. Theory Techn.*, vol. 67, no. 2, pp. 642–658, Feb. 2019.

[26] S. Sancho, A. Suarez, and F. Ramirez, "Envelope domain formulation for the analysis of the nonlinear transient dynamics of coupled oscillators," *IEEE Trans. Microw. Theory Techn.*, vol. 69, no. 1, pp. 566–577, Jan. 2021.

[27] K. Ogata, *Modern Control Engineering*. Upper Saddle River, NJ, USA: Prentice-Hall/PTR, 2001.

[28] V. K. Aatre, *Network Theory and Filter Design*, 2nd ed. New Delhi, India: New Age Int, 1983.

[29] D. Youla, *Theory and Synthesis of Linear Passive Time-Invariant Networks*. Cambridge, U.K.: Cambridge Univ. Press, 2015.

[30] N. B. Buchanan and V. Fusco, "Single VCO chipless RFID near-field reader," *Electron. Lett.*, vol. 52, no. 23, pp. 1958–1960, Nov. 2016.

[31] F. Ramírez, S. Sancho, M. Pontón, and A. Suárez, "Two-scale envelope-domain analysis of injected chirped oscillators," *IEEE Trans. Microw. Theory Techn.*, vol. 66, no. 12, pp. 5449–5461, Dec. 2018.

[32] A. Suarez, R. Melville, and F. Ramirez, "Analysis and synthesis of hysteresis loops in an oscillator frequency characteristic," *IEEE Trans. Microw. Theory Techn.*, vol. 67, no. 12, pp. 4890–4904, Dec. 2019.

[33] F.-K. Wang, T.-S. Horng, K.-C. Peng, J.-K. Jau, J.-Y. Li, and C.-C. Chen, "Single-antenna Doppler radars using self and mutual injection locking for vital sign detection with random body movement cancellation," *IEEE Trans. Microw. Theory Techn.*, vol. 59, no. 12, pp. 3577–3587, Dec. 2011.

[34] S. H. Yu and T. S. Horng, "Highly linear phase-canceling self-injection-locked ultrasonic radar for non-contact monitoring of respiration and heartbeat," *IEEE Trans. Biomed. Circuits Syst.*, vol. 14, no. 1, pp. 75–90, Feb. 2020.

[35] W. C. Su, M. C. Tang, R. El Arif, T. S. Horng, and F. K. Wang, "Stepped-frequency continuous-wave radar with self-injection-locking technology for monitoring multiple human vital signs," *IEEE Trans. Microw. Theory Techn.*, vol. 67, no. 12, pp. 5396–5405, Dec. 2019.

[36] A. Suárez, F. Ramírez, and S. Sancho, "Stability and noise analysis of coupled-oscillator systems," *IEEE Trans. Microw. Theory Techn.*, vol. 59, no. 4, pp. 1032–1046, Apr. 2011.

[37] J. Long, M. M. Jacob, and D. F. Sievenpiper, "Broadband fast-wave propagation in a non-Foster circuit loaded waveguide," *IEEE Trans. Microw. Theory Techn.*, vol. 62, no. 4, pp. 789–798, Apr. 2014.

[38] J. Long and D. F. Sievenpiper, "Stable multiple non-Foster circuits loaded waveguide for broadband non-dispersive fast-wave propagation," *Electron. Lett.*, vol. 50, no. 23, pp. 1708–1710, Nov. 2014.

[39] H. Mirzaei and G. V. Eleftheriades, "Arbitrary-angle squint-free beamforming in series-fed antenna arrays using non-Foster elements synthesized by negative-group-delay networks," *IEEE Trans. Antennas Propag.*, vol. 63, no. 5, pp. 1997–2010, May 2015.

[40] E. Ugarte-Munoz, S. Hrabar, D. Segovia-Vargas, and A. Kiricenko, "Stability of non-Foster reactive elements for use in active metamaterials and antennas," *IEEE Trans. Antennas Propag.*, vol. 60, no. 7, pp. 3490–3494, Jul. 2012.

[41] S. R. Rengarajan and C. R. White, "Stability analysis of superluminal waveguides periodically loaded with non-Foster circuits," *IEEE Antennas Wireless Propag. Lett.*, vol. 12, pp. 1303–1306, 2013.

[42] A. M. Elfrgani and R. G. Rojas, "Stabilizing non-Foster-based tuning circuits for electrically small antennas," in *Proc. IEEE Antennas Propag. Soc. Int. Symp.*, 2014, pp. 464–465.

[43] S. D. Stearns, "Circuit stability theory for non-Foster circuits," in *IEEE MTT-S Int. Microw. Symp. Dig.*, 2013, pp. 1–3.

[44] J. G. Linvill, "Transistor negative-impedance converters," *Proc. IRE*, vol. 41, no. 6, pp. 725–729, Jun. 1953.

[45] C. Kuo, "Realization of negative-immittance converters and negative resistances with controlled sources," Georgia Inst. Technol., Atlanta, GA, USA, 1967.

[46] S. E. Sussman-Fort and R. M. Rudish, "Non-Foster impedance matching of electrically-small antennas," *IEEE Trans. Antennas Propag.*, vol. 57, no. 8, pp. 2230–2241, Aug. 2009.

[47] J. Guckenheimer and P. J. Holmes, *Nonlinear Oscillations, Dynamical Systems, and Bifurcations of Vector Fields (Applied Mathematical Sciences, 42)*. New York, NY, USA: Springer, 1983.

[48] J. M. Thompson and H. B. Stewart, *Nonlinear Dynamics and Chaos*, 2nd ed. West Sussex, U.K.: Wiley, 2002.

[49] S. Hernandez and A. Suarez, "Systematic methodology for the global stability analysis of nonlinear circuits," *IEEE Trans. Microw. Theory Techn.*, vol. 67, no. 1, pp. 3–15, Jan. 2019.

[50] S. Hernández, M. Pontón, and A. Suárez, "Simulation method for complex multivalued curves in injection-locked oscillators," *IEEE Trans. Microw. Theory Techn.*, vol. 65, no. 11, pp. 4046–4062, Nov. 2017.

[51] J. de Cos, A. Suarez, and J. A. Garcia, "Hysteresis and oscillation in high-efficiency power amplifiers," *IEEE Trans. Microw. Theory Techn.*, vol. 63, no. 12, pp. 4284–4296, Dec. 2015.

[52] J. de Cos and A. Suárez, "Efficient simulation of solution curves and bifurcation loci in injection-locked oscillators," *IEEE Trans. Microw. Theory Techn.*, vol. 63, no. 1, pp. 181–197, Jan. 2015.

[53] H. G. Brachtendorf, R. Melville, P. Feldmann, S. Lampe, and R. Laur, "Homotopy method for finding the steady states of oscillators," *IEEE Trans. Comput.-Aided Design Integr. Circuits Syst.*, vol. 33, no. 6, pp. 867–878, Jun. 2014.

[54] Advanced Design System (ADS), Keysight Technologies, Santa Rosa, CA, USA.

[55] H.-C. Chang, "Phase noise in self-injection-locked oscillators - Theory and experiment," *IEEE Trans. Microw. Theory Techn.*, vol. 51, no. 9, pp. 1994–1999, Sep. 2003.

[56] H.-C. Chang, "Stability analysis of self-injection-locked oscillators," *IEEE Trans. Microw. Theory Techn.*, vol. 51, no. 9, pp. 1989–1993, Sep. 2003.

[57] W. S. Chang and C. Y. Chang, "A high slow-wave factor microstrip structure with simple design formulas and its application to microwave circuit design," *IEEE Trans. Microw. Theory Techn.*, vol. 60, no. 11, pp. 3376–3383, Nov. 2012.

[58] J. Selga, P. Vélez, J. Bonache, and F. Martin, "High miniaturization potential of slow-wave transmission lines based on simultaneous inductor and capacitor loading," in *Proc. 47th Eur. Microw. Conf. (EuMC)*, Dec. 2017, pp. 783–786.

[59] M. Pontón, F. Ramírez, A. Herrera, and A. Suárez, "Oscillator stabilization through feedback with slow wave structures," *IEEE Trans. Microw. Theory Techn.*, vol. 68, no. 6, pp. 2358–2373, Jun. 2020.

[60] B.-j. Jang, B.-j. Jang, S.-h. Wi, J.-g. Yook, M.-q. Lee, and K.-j. Lee, "Wirelesss bio-radar sensor for heartbeat and respiration detection," *Prog. Electromagn. Res.*, vol. 5, pp. 149–168, 2008.

[61] J. M. Paillot, J. C. Nallatamby, M. Hessane, R. Quere, M. Prigent, and J. Rousset, "A general program for steady state, stability, and FM noise analysis of microwave oscillators," in *IEEE MTT-S Int. Microw. Symp. Dig.*, 1990, vol. 3, pp. 1287–1290.

[62] V. Rizzoli, F. Mastri, and D. Masotti, "General noise analysis of nonlinear microwave circuits by the piecewise harmonic-balance technique," *IEEE Trans. Microw. Theory Techn.*, vol. 42, no. 5, pp. 807–819, May 1994.

ALMUDENA SUÁREZ (Fellow, IEEE) was born in Santander, Spain. She received the Licentiate degree in electronic physics and the Ph.D. degree from the University of Cantabria, Santander, Spain, in 1987 and 1992, respectively, and the Ph.D. degree in electronics from the University of Limoges, Limoges, France, in 1993. She is currently a Full Professor with University of Cantabria, Spain and Head of the Research Group Microwave Engineering and Radiocommunication Systems. She was an IEEE Distinguished Microwave Lecturer during 2006–2008. She has authored the book *Analysis and Design ofAutonomous Microwave Circuits* (IEEE-Wiley, 2009) and coauthored the book *Stability Analysis of Nonlinear Microwave Circuits* (Artech House, 2003).

Prof. Suárez is a member of the Technical Committees of the IEEE International Microwave Symposium (IEEE MTT-S) and the European Microwave Week. She was a member of the Board of Directors of the European Microwave Association between 2012 and 2020 and is at present the Publication Officer of this association. She was the Coordinator of the Communications and Electronic Technology Area for the Spanish National Evaluation and Foresight Agency (ANEP) between 2009 and 2013. She was the Chair of the 2014 and 2015 editions of the IEEE Topical Conference on RF/Microwave Power Amplifiers (PAWR), in Newport Beach and San Diego. She was the General TPC Chair of the European Microwave Week 2018. She was the Editor-in-Chief of the *International Journal of Microwave and Wireless Technologies* from Cambridge University Press journals from 2013 to 2018 and is currently an Associate Editor for IEEE MICROWAVE MAGAZINE and IEEE TRANSACTIONS ON MICROWAVE THEORY AND TECHNIQUES.

SERGIO SANCHO (Member IEEE) received the degree in physics from Basque Country University in 1997. In 1998, he joined the Communications Engineering Department of the University of Cantabria, Spain, where he received the Ph.D. degree in electronic engineering in February 2002. Currently, he works with the University of Cantabria, as an Associate Professor with the Communications Engineering Department. His current research interest is focused on the nonlinear analysis of microwave autonomous circuits and systems, including the study of their stability and behavior in the presence of stochastic signals like noise and modulation.

FRANCO RAMÍREZ (Senior Member, IEEE) received the Licentiate degree in electronic systems engineering degree from the Military School of Engineering (EMI), La Paz, Bolivia, in 2000 and the Ph.D. degree in communications engineering from the University of Cantabria, Santander, Spain in 2005. From 1999 to 2000, he worked for Ericsson de Bolivia Telecomunicaciones, where he was involved in projects related with GSM and TDMA technologies. From 2009 to 2013, he was a Research Fellow of the "Ramón y Cajal" Programme, funded by the Spanish Ministry of Science and Innovation, at the Communications Engineering Department of the University of Cantabria, where he is currently an Associate Professor. His research interests include phase noise, stability and the development of nonlinear techniques for the analysis and design of autonomous microwave circuits.

MABEL PONTÓN (Member, IEEE) was born in Santander, Spain. She received the bachelor's degree in telecommunication engineering, the master's degree in information technologies and wireless communications systems, and the Ph.D. degree from the University of Cantabria, Santander, in 2004, 2008, and 2010, respectively. In 2006, she joined the Communications Engineering Department, University of Cantabria.

From 2011 to 2013, she was with the Group of Electronic Design and Applications, Georgia Institute of Technology, Atlanta, GA, USA, as a Postdoctoral Research Fellow. Her current research interests include the nonlinear analysis and simulation of radiofrequency and microwave circuits, with an emphasis on phase-noise, stability, and bifurcation analysis of complex oscillator topologies.